Submicron and Nanometer Structures

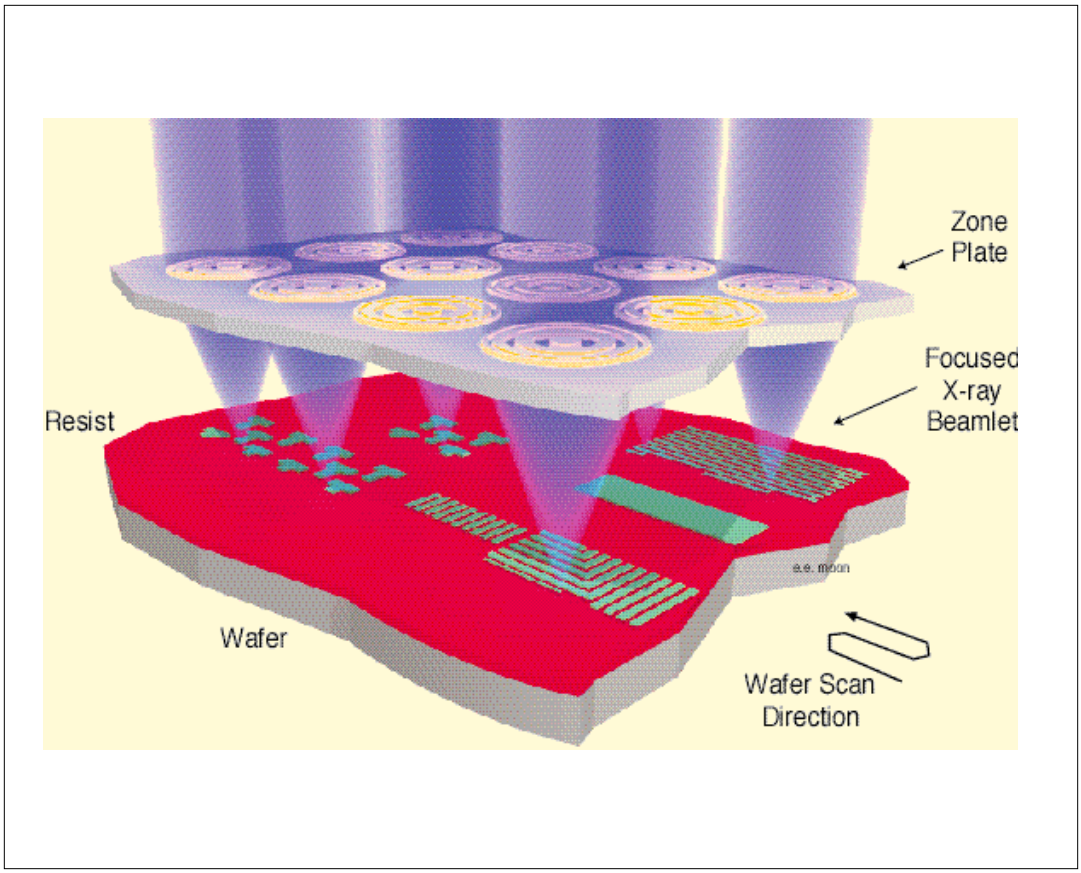

Schematic of a maskless projection lithography scheme that employs 4.5 nm x-rays focused to an array of diffraction-limited spots. Writing is done via a dot-matrix scheme, with micromechanical shutters modulating the x-ray flux to each zone plate. With 4.5 nm x-rays, 25-nm or smaller spot sizes should be attainable. (Courtesy of H. I. Smith)

Submicron and Nanometer Structures

- *Interferometric Lithography*
- *Scanning-Electron-Beam Lithography*
- *Spatial-Phase-Locked Electron-Beam Lithography*
- *X-Ray Nanolithography*
- *Improved Mask Technology for X-Ray Lithography*
- *Zone-Plate-Based X-Ray and UV Projection Lithography*
- *Magnetic Materials for Data Storage*
- *Ultra-small Gate Aperture Field Emitter Arrays using Interference Lithography*
- *Low Voltage Field Emission Displays for Head-Mounted Applications*
- *High-Dispersion, High Efficiency Transmission Gratings for Astrophysical X-ray Spectroscopy*
- *Transmission Gratings as UV-blocking Filters for Neutral Atom Imaging*
- *Super-smooth X-ray Reflection Gratings*
- *Submicron-Period Transmission Gratings for X-ray and Atom-Beam Spectroscopy and Interferometry.*

Interferometric Lithography

Personnel

J. M. Carter, M. Farhoud, J. Ferrera, R. C. Fleming, T. A. Savas, M. Walsh (M. L. Schattenburg and H. I. Smith)

Sponsorship

ONR, AFOSR, and ARO

Interferometric lithography is preferred for the fabrication of periodic and quasi-periodic patterns that must be spatially coherent over large areas. For spatial periods down to 200 nm, an argon ion laser is used in a Mach-Zehnder configuration, with a fringe-locking feedback system, as illustrated in Figure 1. This scheme produces large area (10-cm diameter) gratings with long-range, spatial-phase coherence. Fringe locking ensures reproducibility of exposure.

The gratings and grids produced are used as fiducials in spatial-phase-locked electron-beam lithography and in a new approach to metrology for the sub-100 nm domain. In addition, a wide variety of applications, from ultra-high-density magnetic information storage to atom-beam interferometry, depend on interferometrically produced grainges and grids. These applications are separately described in this report.

For spatial periods below 200 nm, a source wavelength below 200 nm must be used. Since such sources have limited temporal coherence, one is forced to employ an achromatic scheme, as shown in Figure 2. The source is an ArF laser (193 nm wavelength). A collimating lens, polarizer and scanning system are interposed between the source and the interferometer in order to achieve reasonable depth-of-focus and large exposure areas. We also use a white light interference principle to insure equal path lengths in the two interferometer arms. Using this system, gratings and grids of 100 nm perod (nominally 50 nm lines or posts) are obtained in PMMA on top of an antireflection coating. Figure 3 shows a 100 nm-period grid etched into Si following achromatic interferometric lithography. Grids of Si posts are being used to investigate photo-and electroluminescence which may result from charge-carrier quantum confinement.

To obtain spatial periods below 100 nm, a source wavelength below 100 nm and an achromatic scheme must be employed. We have established a collaboration with the University of Wisconsin, in which we will utilize an undulator light source (13 nm wavelength) incorporated into their synchrotron. An achromatic interferometer, currently being designed and built, will be capable of exposing 50-nm period gratings and grids in resist.

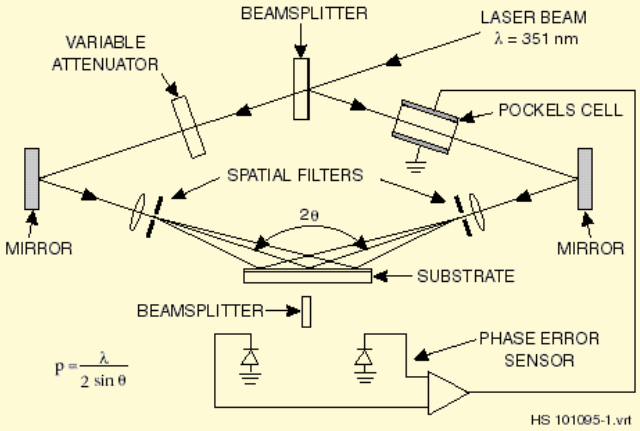

Fig. 1: Schematic of the MIT interferometric lithography system. The system occupies a 2x3m optical bench in a class 100 clean environment. The beamsplitter directs portions of the two interfering spherical beams to photodiodes. A feedback locking is achieved by differentially amplifying the photodiode signals and applying a correction to the Pockels cell which phase shifts one of the beams.

continued

continued

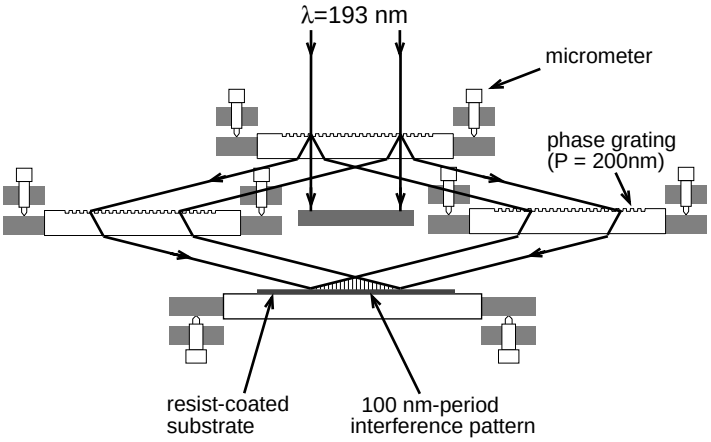

Fig. 2: Achromatic interferometric lithography (AIL) configuration employed to produce 100 nm-period gratings and grids.

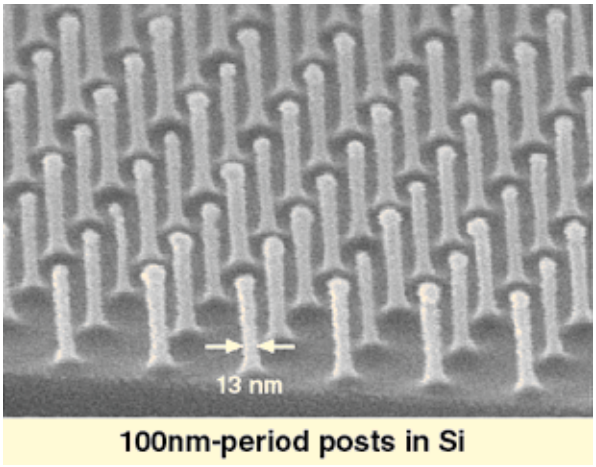

Fig. 3: Scanning electron micrograph of a 100 nm-period grid, exposed in PMMA on top of an antireflection coating, and transferred into Si by reactive ion etching.

continued

Scanning-Electron-Beam Lithography

Personnel

M. K. Mondol (H. I. Smith)

Sponsorship

ARO, AFOSR, DARPA, NSF, SRC through U. C. Berkeley

Figure 4 is a photograph of the scanning-electron-beam lithography system (VS-2A) located in the scanning-electron-beam lithography (SEBL) facility, Room 38-165. This instrument was obtained as a donation from IBM in November 1993. Its digital pattern generator is based on a commercial high-performance array processor, which uses dual RISC processors. The system is capable of creating large-area patterns composed of multiple stitched fields. Conversion software has been developed which allows a CAD data file to be fractured and translated prior to exposure by the electron-beam tool.

The VS-2A can expose substrates up to 20 cm diameter, at linewidths down to 70 nm. The goals of the SEBL facility are to: (1) provide the MIT research community with an in-house SEBL capability for writing directly on experimental device substrates; (2) advance the state-of-the-art in SEBL, particularly with regards to pattern placement accuracy and long-range spatial-phase coherence; and (3) pattern x-ray nanolithography masks for in-house use. In order to enable writing concentric circular patterns, such as Freznel zone plates, software was developed to generate arbitrary arcs of an annulus with user-specified start and finish radii and angles.

In 1998, the VS-2A was used to write: Freznel zone plates, as phase masks, on quartz for experiments in zone-plate-array lithography; 100 nm features on quartz masks for UV contact lithography experiments; gratings for channel-dropping filters, with long range coherence, on x-ray masks; and alignment marks, on x-ray masks, for experiments on IBBI alignment. VS-2A was used in the direct-writing mode for projects on: magnetic storage; a super-luminescent LED using a two dimensional photonic band gap; 1-D photonic bandgap structures; and 3-D photonic bandgap structures (Figure 5). VS-2A was also used extensively in experiments on spatial-phase-locked e-beam lithography.

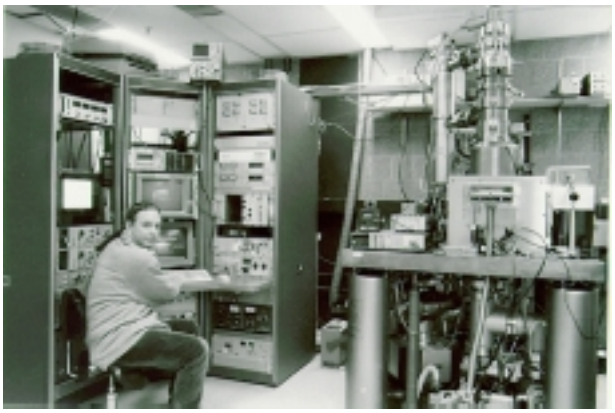

Fig. 4: Photograph of the VS-2A scanning-electron-beam lithography system. The operator is Research Specialist Mark Mondol.

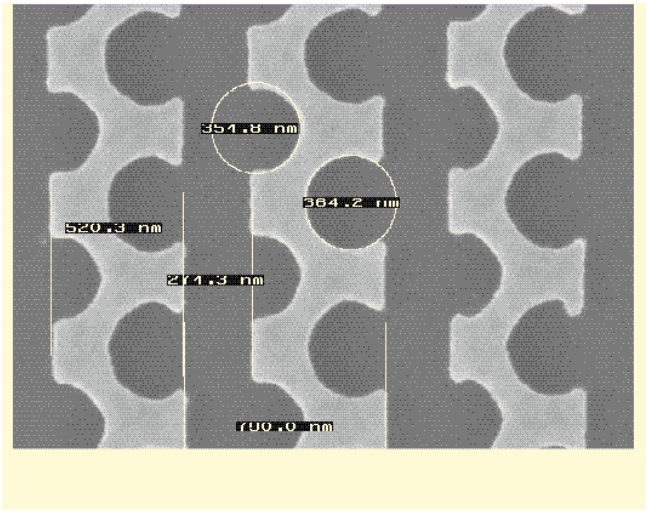

Fig. 5: Scanning-electron micrograph of an early stage in the fabrication of a three-dimensional photonic bandgap (PBG) structure for the 1.5-micron wavelength, written with VS-2A. The micrograph shows the complex geometry and dimensional control necessary for this type of PBG structure. The design, which enables planar nanofabrication technology to be used, was developed in Prof. J. D. Joannopoulos' group.

Spatial-Phase-Locked Electron-Beam Lithography

Personnel

N. Basoco, A. Bernshteyn, J. Ferrera, Dr. J. G. Goodberlet, M. K. Mondol (H. I. Smith)

Sponsorship

ARO, DARPA, SRC through U. C. Berkeley

Spatial-phase-locked electron-beam lithography (SPLEBL) has been under development at MIT for several years, and promises to reduce pattern-placement errors in electron-beam lithography systems to the nanometer level. Such high precision is essential for future integrated electronics and integrated optics. Currently, SPLEBL is the only approach capable of achieving this goal. Nanometer precision in pattern placement is possible by incorporating feedback into the electron-beam lithography system. In SPLEBL, a low-level, periodic signal, derived from the interaction of the e-beam with a fiducial grid on the substrate, is used to continuously track the position of the e-beam while patterns are written. Any deviations of the beam from an intended location are sensed, and corrections are fed back to the beam-control electronics to cancel errors in the beam's position.

Our goal this year has been to extend SPLEBL from an earlier one-dimensional demonstration to a two-dimensional demonstration. To accomplish this, several improvements in SPLEBL components have been required. Specifically, our tasks have been to (1) improve the fiducial grid which is patterned on the substrate and generates the periodic signal, (2) design and build a high-speed electron-beam dose modulator, and (3) develop a digital-signal processing algorithm which phase-locks to the periodic fiducial-grid signal and determines precisely the beam-position corrections.

The fiducial grid for SPLEBL typically provides a weak signal. To improve the signal quality and simplify patterning of the fiducial grid, we have developed a PMMA-based organic, scintillating polymer mixture. The composition, by weight, of the scintillator is PMMA (87%), naphthalene (8%), anthracene (2.5%) and 2,2'-p -phenylenebis-(5-phenyloxazole) (2.5%). PMMA is an electron-beam sensitive resist, and the other components provide the scintillation signal. Anthracene is an ultraviolet-sensitive scintillator, i.e. its scintillation is quenched after exposure to UV radiation, and because of this property a scintillating fiducial grid may be patterned easily in the polymer by exposing it to a UV standing wave. The measured quenching property of this resist-scintillator composition is shown in Figure 6. A signal contrast of 2.8 was measured from a scintillating fiducial grating patterned in this polymer which is a substantial improvement upon the value of contrast (1.15) obtained in the previous demonstration of SPLEBL which employed backscattered electrons. We also observed that the UV irradiation did not affect the e-beam resist's properties. Hence, this polymer formulation incorporates both the e-beam resist and scintillating fiducial grid into a single layer, which is spun onto a substrate for patterning. We are also investigating bi-layer schemes in which the resist and scintillating polymers may be spun onto the substrate separately.

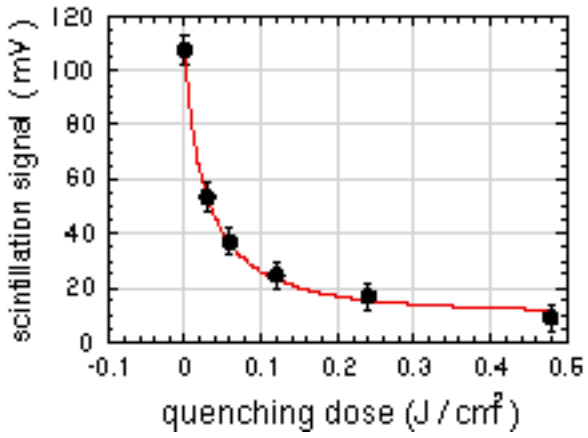

Fig. 6: The quenching response of the scintillator-resist composition was measured after exposing it to 351 nm radiation. This radiation did not affect the electron-beam resist's properties.

continued

In SPLEBL, a high-speed electron-beam dose modulator must be used to switch the e-beam rapidly from a "fully-on" state, when exposing patterns, to a "partly-on" state, when moving between patterns. The "partly-on" state permits continuous monitoring of the e-beam's position, i.e. constant feedback. The dose modulator must be capable of switching in short times, ~ 1 ns, to permit patterning at high data rates. We have designed an electrostatic deflection apparatus (quadra deflector) which enables high-speed dose modulation. The quadra deflector consists of four pairs of deflection plates which locally deviate the electron-beam path between two current-limiting apertures. The quadra deflector is shown in Figure 7, along with a bench-top electron-beam column which is being assembled to test the deflector. In a simple electrical measurement the quadra deflector's plates were switched in 6.0 ns, as shown in the graph of Figure 8. This time was primarily determined by the slow current driver used to switch the plates and cabling between the driver and plates. The response of the plates is calculated to be about 0.75 ns.

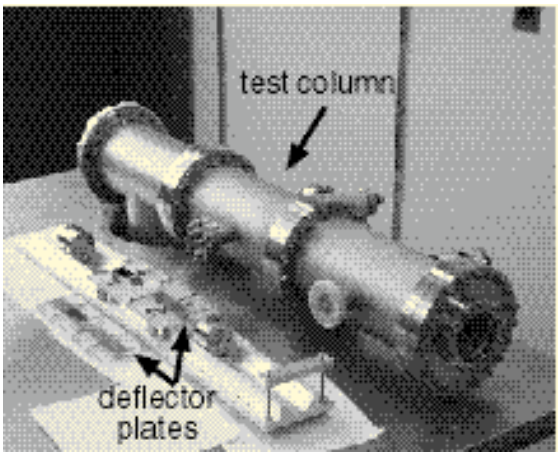

Fig. 7. The quadra-deflection electron-beam dose modulator, shown in the foreground, consists of four electrostatic deflectors and an aperture plate. The quadra deflector will be tested in the bench-top electron-beam column shown in the background.

We are investigating the application of digital-signal processing to the SPLEBL architecture. In the previous proof-of-concept experiment, analog circuitry was used to demonstrate SPLEBL in one dimension. We believe DSP techniques are better suited for the 2-D SPLEBL system because of greater flexibility in feedback algorithms and greatly reduced complexity in circuit design. To develop a robust and efficient DSP algorithm for SPLEBL, we must first develop a realistic model of the electron-beam system and expected fiducial grid signal. This simulated signal, which reflects properties of the organic scintillator and system noise, will be used to test the DSP phase-locking algorithms.

We have begun programming the signal simulator which incorporates such factors as scintillator quenching response, contrast of the UV standing wave used to pattern the fiducial grating, and convolution of the electron-beam profile and fiducial-grid pattern. Two results from the simulator are shown in Figure 9. The graphs show the expected scintillation contrast from two types of organic scintillating fiducial grids. In one case, lower trace, the scintillating polymer has the nonlinear quenching response . For the other case, the quenching response is modeled as linear. Clearly, the linear case is more desirable, and we will investigate ways to improve the quenching response of the scintillator. The signal simulator will be complete when we have added noise, characteristic of the e-beam system, to the signal.

After completing experiments with the dose modulator and testing phase-locking algorithms, we will be ready to demonstrate two-dimensional SPLEBL. We anticipate a demonstration in the coming year.

continued

continued

X-Ray Nanolithography

Personnel

Dr. D. J. D. Carter, J. M. Daley, M. H. Lim, E. E. Moon
(H. I. Smith)

Sponsorship

DARPA / U.S. Navy – Naval Air Systems Command

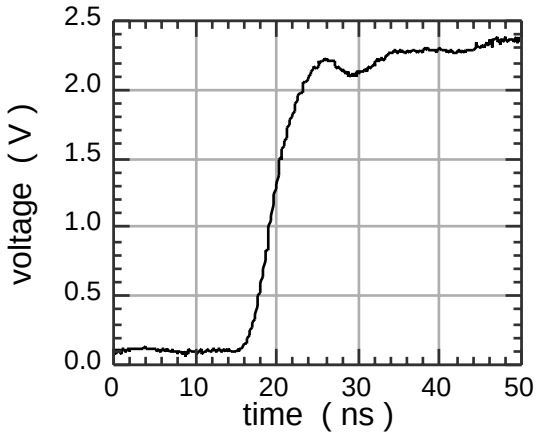

Fig. 8 The electrical switching time of the quadra deflector's plates were measured to be about 6.0 ns. This risetime was primarily determined by the current driver, about 4.7 ns, and cabling used to connect the plates and driver. The calculated switching time for the plates is about 0.75 ns.

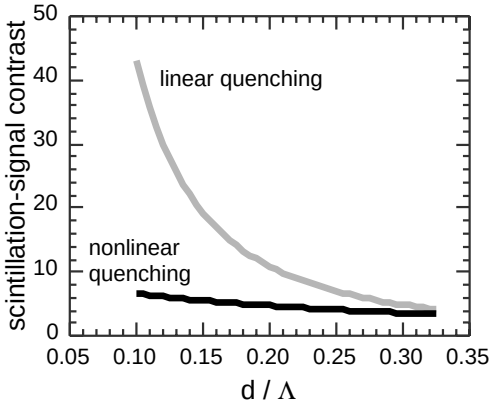

Fig. 9. The contrast expected from a scintillating fiducial grid with a linear quenching response is better than that from our existing polymer formulation. The graph was generated using a signal simulator that is being developed to test DSP phase-locking algorithms for SPLEBL.

For several years, we have been developing the tools and methods of x-ray nanolithography. We have explored the theoretical and practical limitations, and endeavored to make its various components (e.g. mask-making, resists, electroplating, sources, alignment, etc.) reliable and "user-friendly." Because of the critical importance of x-ray mask technology, we discuss this in a separate section.

Our sources for x-ray nanolithography are simple, low-cost electron-bombardment targets, typically Cu_L (λ= 1.32 nm), separated by a 1.4 μm-thick SiN_x vacuum window from a helium-filled exposure chamber. In the future, we hope to replace the Cu_L sources with a higher-flux plasma-focus source.

In earlier research, we showed that for wavelengths longer than 0.8 nm, the important limit on resolution is diffraction in the gap between mask and substrate. With a CuL source, a 50 nm feature must be exposed at a mask-to-substrate gap of less than about three microns in order to maintain good process latitude. A 25 nm feature would require a gap of less than a micron. For very small features, we eliminate the gap and use contact between the substrate and the flexible membrane mask, induced by electrostatic forces or partial vacuum and atmospheric pressure. This technique has allowed us to replicate features as small as 25 nm in size in a practical reproducible way. Figure 10 shows scanning electron micrographs of device pattern replication by liftoff onto a substrate with feature sizes less than 40 nm. The x-ray mask is shown on top and the lifted-off pattern is on the bottom.

To create the x-ray masks, the pattern is first written by electron-beam lithography onto an x-ray "mother" mask, using either our in-house e-beam system or in a collaboration with the Naval Research Laboratory in Washington, DC. The e-beam written pattern is developed, and gold is electroplated into the resist mold. A

negative replica, or "daughter" mask is created by exposing with the mother mask using soft-contact x-ray nanolithography. Finally, the daughter mask is exposed onto the device substrate.

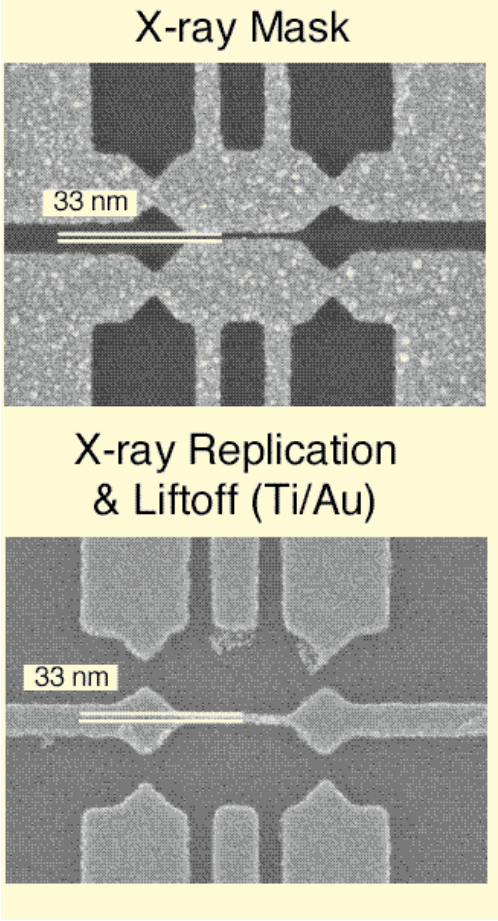

Fig. 10: Scanning electron micrographs of device pattern replication by liftoff onto a substrate with feature sizes less than 40 nm. The x-ray mask is shown on top and the lifted-off pattern is on the bottom.

Recent work has focused on investigating process latitude at these extremely fine feature sizes. Figure 11 shows how developed linewidth changes for up to 50% overdevelopment (i.e. developing for 50% longer than it takes for the feature to clear) as a function of linewidth. As can be seen from the plot, the measured feature on the substrate remains within a +/- 10% process window (within the accuracy of the measurement) for isolated features as small as 30 nm and for dense features (greater than 1:3 line:space ratio) as small as 45 nm. This data indicates that soft-contact x-ray lithography is extremely robust and offers very wide process latitude.

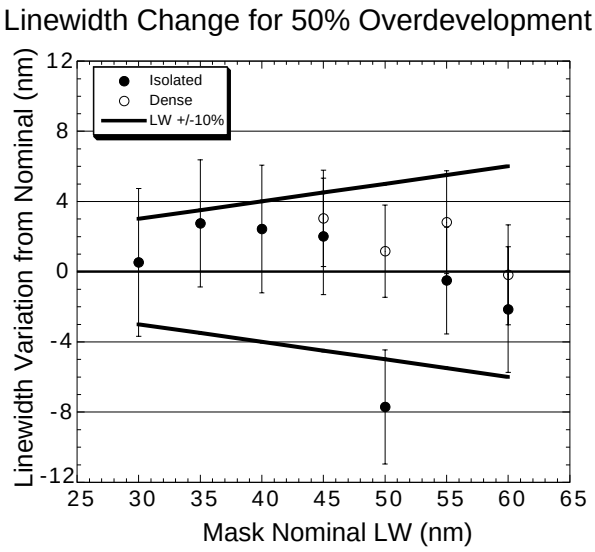

Fig. 11: Plot of linewidth varation from nominal (i.e. developed for the time required to clear features) for up to 50% overdevelopment. Isolated features stay within a +/-10% process window for features as small as 30 nm. Dense (line:space ratio of 1:3 or greater) features remain in the process window for features as small as 45 nm.

Improved Mask Technology for X-Ray Lithography

Personnel

J. M. Daley, J. Ferrera, M. H. Lim, K. Murooka, E. R. Murphy, K. P. Pipe (H. I. Smith)

Sponsorship

DARPA/Naval Air Systems Command

At feature sizes of 100 nm and below the mask-to-substrate gap, G, must be less than ~10 μm . Thus, for nanolithography the mask membrane should be considerably flatter than 1 μm, preferably ~100 nm. Our mask technology is based on low-stress, Si-rich silicon nitride, SiN_x. This material is produced in a vertical LPCVD reactor. Membranes of SiN_x can be cleaned and processed in conventional ways. For absorber patterns we electroplate gold onto the membrane, using a specially designed apparatus, after resist exposure and development. A Ti/Au plating base is deposited on the membrane prior to resist coating. To pattern periodic structures on the x-ray masks, we use interferometric lithography (IL) and for patterns of arbitrary geometry, we use e-beam lithography—either at the MIT SEBL facility or in collaboration with NRL. We use our Leo SEM and Digital Instruments STM/AFM to inspect our x-ray masks for defects. Radiation hardness for SiN_x membranes remains a problem at dose levels corresponding to production (i.e., millions of exposures). For research purposes, however, the material is entirely acceptable.

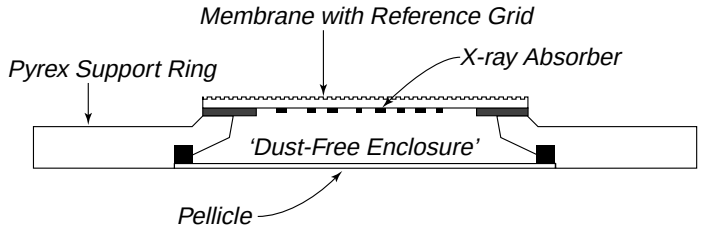

Fig. 12: Schematic showing how the absorber pattern on an x-ray mask can be protected from the accumulation of dust and other contamination by enclosing it between the membrane and a pellicle. Dust accumulated on the membrane can be removed by aggressive techniques. The grid is to enable measurement of in-plane distortion via the HPSI interferometer (Fig. 14)

Currently we are developing a pellicled x-ray mask, depicted in Figure 12, which has several advantages over the traditional x-ray mask: (1) the critical absorber pattern can be protected within a dust-free enclosure; (2) the membrane can be cleaned using aggressive techniques without damaging the absorber pattern; (3) any dust that falls onto the pellicle will not be imaged onto the substrate due to diffraction and penumbral blurring; (4) the resulting membranes are flat to less than 30 nm, as shown in Figure 13; (5) one can place a fiducial grid on the frontside of the membrane to track distortions that might occur during the processing and lifetime of the mask. To fully take advantage of this x-ray mask configuration, we must be able to anodically bond the membrane to the mask frame with minimal distortion.

To analyze the distortions that occur during the anodic bonding of the membrane to the pyrex ring, we have developed a broadly applicable, nondestructive, global, membrane-distortion measurement technique. This technique uses a holographic phase-shifting interferometer (HPSI) based on the apparatus that Ferrera et al used to measure the phase distortion of interferometrically-generated gratings.

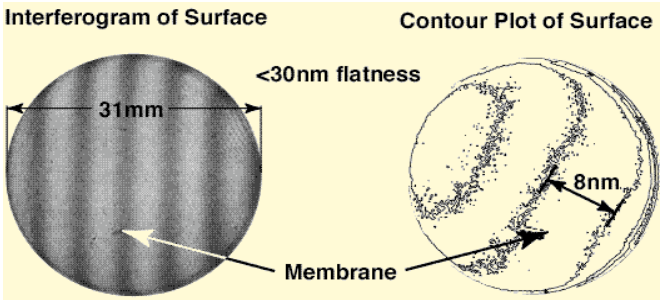

flatness better than ~30 nm over most of the membrane area.

The HPSI system is based on the interferometric lithography (IL) system we use to generate large-area, highly-coherent gratings. Figure 14 is a schematic of the IL apparatus, configured as a HPSI system. The IL system splits a laser beam (λ=351nm) and forms two mutually coherent spherical waves, which interfere at the substrate at a half-angle θ. The standing wave created at the substrate surface is used to expose photoresist. After development, the grating is present on the substrate surface or can be etched into it. The IL system is configured as a holographic interferometer simply by mounting the IL-generated grating on the substrate platform and placing a fluorescent screen in front of one of the spatial filters, as depicted in Figure 14. A fringe pattern appears on the screen, which is due to the superposition of two wave fronts: one reflected from the substrate surface and the other back-diffracted from the grating. If the grating has suffered no distortion between exposure and reinsertion, the reflected and back-diffracted beams will be identical and no fringes will be observed on the screen. Any in-plane distortion of the grating will result in a fringe pattern. A CCD camera is used to capture the fringes. To increase the precision, a phase-shifting measurement is implemented, by changing the phase of one of the arms and acquiring several images. In order to use this apparatus to measure the in-plane distortion, we etch shallow IL-generated gratings into the membrane.

We first form a membrane that is 54 mm in diameter and 1 μm thickness. Next we pattern 400 nm period gratings into a number of membranes, including one that we set aside as a reference. Then we anodically bond these membranes to pyrex frames, except for the reference membrane. Afterwards, we place the reference membrane into the HPSI system and align the system so that it exactly matches the conditions that previously exposed the grating; good alignment is ensured by minimizing the number of fringes in the interference pattern. Finally, we

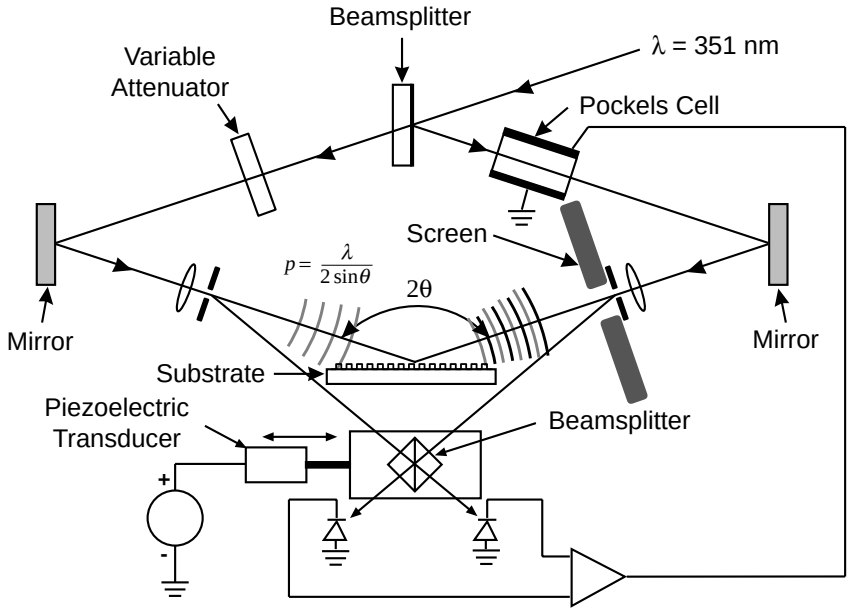

Fig. 14: A schematic of the Holographic Phase-Shifting Interferometer (HPSI) based on the interferometric lithography system that we use to generate highly-coherent gratings.

place the flip-bonded x-ray mask into the HPSI system and acquire an interferogram; we then analyze the interferogram using the 5-step Hariharan algorithm. The process flow for the measurement is shown in Figure 15. A typical interferogram is shown in Figure 16a. Analysis of this data indicates that the period of the grating contracted from 400nm to 399.97 nm. Figure 16b shows a one-dimensional distortion plot extracted from the interferogram. As a check we measured the period contraction using a different method. The half-angle of recombination of both beams can be changed by translating the substrate in the direction perpendicular to its surface; a positive translation shortens the period of the standing wave. We employed this effect to directly measure the period change of the grating by translating the substrate stage forward until the fringes were minimized. After moving the stage forward by 130 μm, the fringes were minimized, indicating that the period of the distorted grating was 399.97 nm which agrees with the value extracted from the interferogram analysis. We are currently working to extend the measurement system to two-dimensions as well as attempting to minimize the distortion caused by anodic bonding.

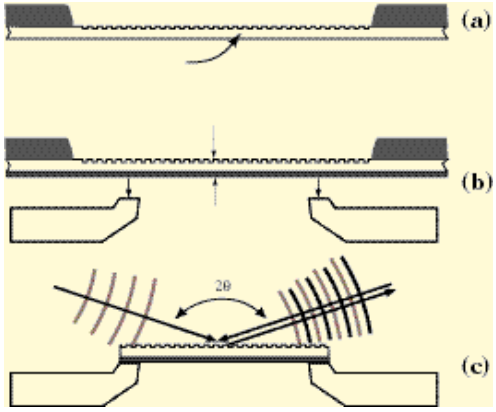

Fig. 15: The process used for measuring the distortion that occurs during anodic bonding: (a) a 400nm period grating is etched into the membrane; (b) the membrane is bonded to a pyrex frame; (c) the completed mask is placed in the HPSI for analysis.

Fig. 16: Measurement and analysis results from the HPSI; (a) the interferogram that results when the completed mask is placed back into the HPSI; (b) the distortion map calculated from (a) showing the grating contraction and the resulting in-plane distortion due to the anodic bonding.

Zone-Plate-Based X-Ray and UV Projection Lithography

Personnel

Dr. D. J. D. Carter, D. Gil, R. Menon (H. I. Smith)

Sponsorship

DARPA, SRC through U. C. Berkeley

Soft-contact x-ray nanolithography is unique to MIT, and although suitable for research, it is considered incompatible with manufacturing. Accordingly we are developing an alternative approach that would preserve the desirable features of x-ray lithography while circumventing the need to bring the mask into intimate contact with the substrate. Our proposed solution, Zone-Plate Array Lithography (ZPAL), is a maskless projection lithography system that employs an array of Fresnel zone plates. As illustrated in Figure 17, an array of Fresnel zone plates focuses an incident beam of 4.5 nm x-rays, forming an array of diffraction-limited spots on a substrate. Writing is done via a dot-matrix-printing strategy, with the individual beams multiplexed by an array of micromechanical shutters located upstream of the zone-plate array. The resolution or spot size is approximately equal to the width of the outermost zone. Hence, the resolution of the system is determined by one's ability to make the zone plates by e-beam lithography and dry etching. The maskless projection system, shown in Figure 17, would eliminate the need for a mask, potenetially decreasing the overall cost of ultra-fine lithography. Moreover, for patterning at the limits of the lithographic process, the 4.5 nm photon offers the optimal combination of minimal proximity effects, short enough wavelength to enable large depth-of-focus, and sufficient penetration to eliminate the need for surface-interaction resists. Although the best available source of 4.5 nm photons with the necessary temporal and spatial coherence is an undulator attached to a synchrotron, we are using a C_K ($\lambda = 4.5$ nm) electron bombardment source for purposes of research. With this source we intend to prove the resolution limits of ZPAL.

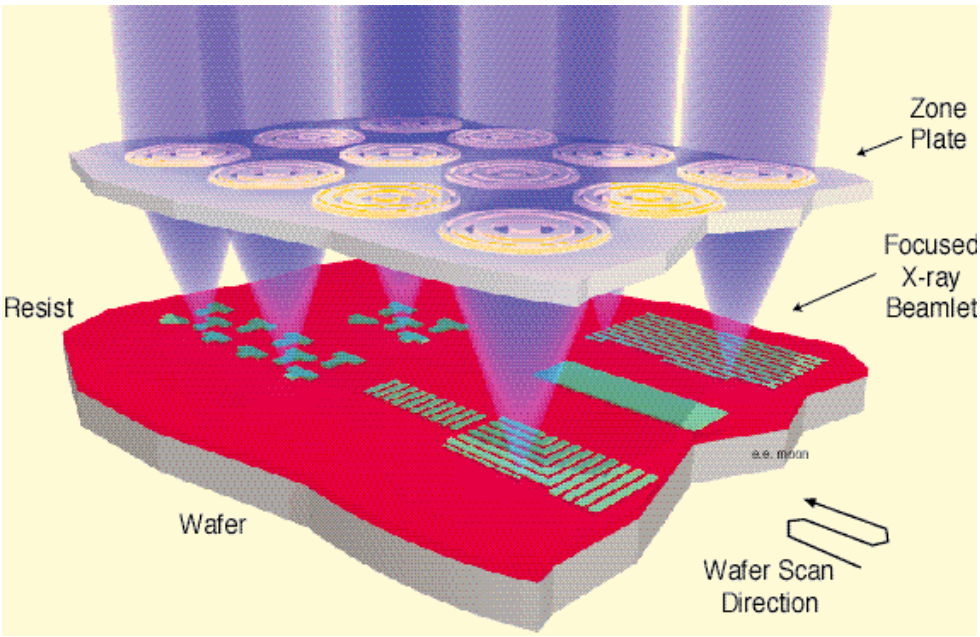

Fig.17: Schematic of a maskless projection lithography scheme that employs 4.5 nm x-rays focused to an array of diffraction-limited spots. Writing is done via a dot-matrix scheme, with micromechanical shutters modulating the x-ray flux to each zone plate. With 4.5 nm x-rays, 25-nm or smaller spot sizes should be attainable.

continued

continued

At the same time, to explore system design issues, an experimental UV ZPAL system has been constructed. We have fabricated phase-shifting zone plates in quartz and built an apparatus that ensures the substrate is in the correct focal plane of the zone plate array. With this setup the results shown in Figure 18 were obtained. Since then, we have added multiplexing capabilities to the system by means of an array of commercially available Texas Instruments micromechanical reflecting mirrors, with promising preliminary results. With the acquisition of a sub-4 nm precision stage we should be able to expose arbitrary patterns that extend among many zone plate unit cells. This UV system, in addition to providing maskless lithography capabilities, should be a good proving ground for multiplexing and stage coordination issues for x-ray ZPAL.

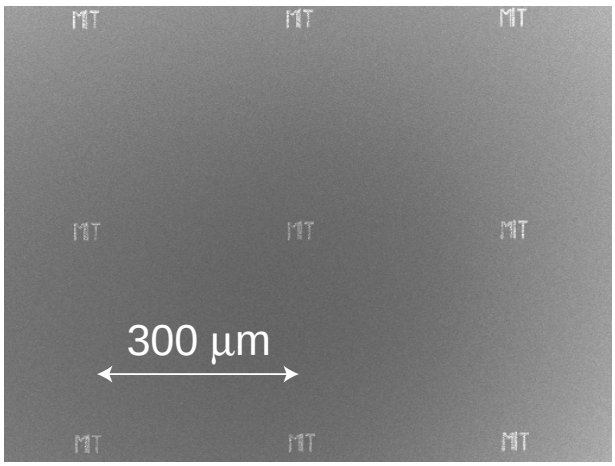

Fig. 18: Scanning electron micrograph of a pattern in PMMA after development. The 3 x 3 array of patterns were written in parallel with a zone-plate array focusing the deep-UV radiation from an ArF laser (λ = 193 nm). For this example, the stage was moved by hand and no multiplexing was performed.

Magnetic Materials for Data Storage

Personnel

M. Farhoud, Y. Hao, M. Hwang, M. E. Walsh, T. Savas, Y. Shine and D. Twisselmann (C. A. Ross, H. I. Smith)

Sponsorship

NSF, DARPA, IBM Graduate Fellowship, Department of Materials Science and Engineering

As hard disk recording densities increase, the grain size of the magnetic layer is being reduced in order to maintain a good signal/noise ratio when reading data from the disk. However, if the grains become too small then a 'superparamagnetic' limit is reached in which the magnetization direction in the magnetic grains can be reversed by thermal energy, leading to loss of recorded data. One method for reducing media noise is to store data in periodic arrays of 'nanomagnets', lithographically defined magnetic particles, each of which has dimensions of less than 100 nm. Each particle is magnetised in one of two possible directions, representing a 1 or a 0. These nanomagnets also have potential applications as data storage elements in MRAMs, magnetic random access memories, in which data are stored in small magnetoresistive elements.

We are using interferometric lithography in the NanoStructures Laboratory of the Department of Electrical Engineering to produce arrays of nanomagnets of period 100 - 200nm. The particles are formed by electrodeposition, by evaporation and liftoff, or by etching of a previously deposited film. We are exploring the switching mechanisms of the particles, the thermal stability of their magnetization, and interparticle interactions, and assessing their suitability for various data storage schemes (See *Electronic Devices* section, p. 94).

We are also exploring magnetic anisotropy in conventional hard-disk media. Magnetic CoCrTa or CoCrPt films on a Cr underlayer are used in hard disks to store data. The films are deposited at temperatures of 200°C or over, which causes the b.c.c. Cr to grow with a (200) crystallographic texture. The hexagonal Co alloy grows epitaxially on the Cr with a (11.0) texture, putting its c-axis parallel to the film plane. In such films, the presence of substrate roughness has significant effects on in-plane magnetic anisotropy. In particular, the presence of grooves or scratches in the substrate causes the coercivity, remanence and squareness of the film to be considerably higher parallel to the grooves compared to their values in the perpen-

continued

continued

dicular direction. This effect is useful in hard disks, but the physical origin of this anisotropy is still debated. It may be due to in-plane stress differences between the circumferential and radial directions, due to preferential orientation of the c-axes of the Co alloy grains along the grooves, or due to differences in magnetostatic coupling.

We are measuring the anisotropy in films deposited onto oxidised silicon substrates with well-controlled submicron surface topography, to explore the origins of the effect and to demonstrate how it can be enhanced by choice of substrate features. We have been successful in growing (200) Cr/ (11.0) CoCrPt bilayer films with in-plane anisotropy on these substrates, and have shown that internal stress in the films appears to be too small to account for the entire anisotropy. Fig. 19 shows a hysteresis loop from a grooved sample with an anisotropy of 1.6 10^5 erg/cm^3.

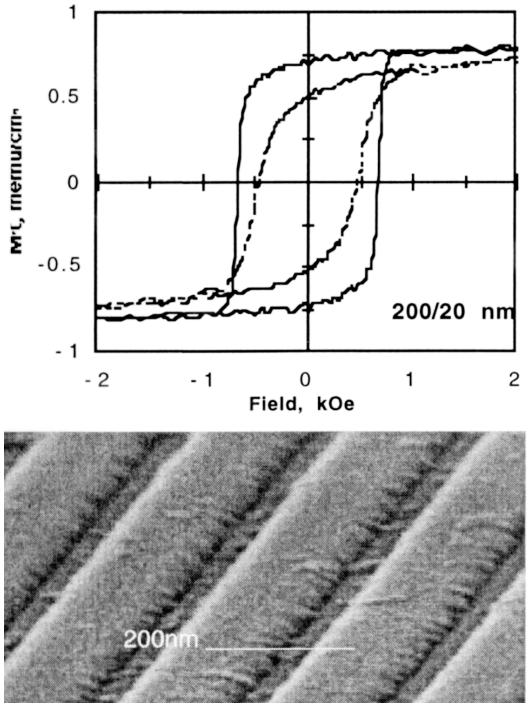

Fig. 19. Magnetic hysteresis loops (top) from a sample (bottom) of Cr/CoCrPt sputtered onto a substrate with 200 nm period, 20 nm deep grooves. Coercivity, remanence and squareness are higher parallel to the grooves (solid line) compared to perpendicular (dotted).

Ultra-small Gate Aperture Field Emitter Arrays using Interference Lithography

Personnel

J. O. Choi and D. Pflug
(A. I. Akinwande in collaboration with H. I. Smith)

Sponsorship

IAE

The goal of this project is to fabricate 100 nanometer gate aperture field emitter arrays (FEAs) using interference lithography (IL). Our approach is to use IL as the critical lithography to define the gate aperture. The expected advantages of fabricating ultra-small gate aperture FEAs using IL are (a) gate apertures as small as 100 nm can easily be defined over a large field size without a mask, (b) FEA pixel size can become smaller because of higher packing density (≈ 2.5 x 10^9 tips cm^{-2}), (c) a reduction in the operating voltage, and (d) a reduction in the stored energy between the electrodes because of the lower operating voltage.

A new process and a mask set (4 masks) for fabricating a matrix addressed 100-nm gate aperture FEAs was developed. Independently matrix-addressable FEAs with various pixel sizes with VGA and SVGA resolution were fabricated. Our device characterization indicates very low turn-on voltage of about 15 volts, however the devices exhibit significant gate leakage current. The source of the leakage current is under investigation.

Low Voltage Field Emission Displays for Head-Mounted Applications

Personnel

D. Pflug (A. I. Akinwande in collaboration with Dr. M. Schattenburg, and Prof. H. I. Smith)

Sponsorship

DARPA

Field emitter arrays fabricated by interference lithography are being explored for small, high resolution, high luminous efficiency and high brightness image sources for Head-Mounted Displays (HMDs). The image sources incorporate a high density, high performance array of low voltage field emitters as two dimensional array of electron sources for a cathodoluminscent screen. The initial objective of this project is to demonstrate that 100 nm gate aperature FEAs have low operating voltages and to explore the scaling rules for FEAs.

FEAs of 200 nm period have been fabricated using the interferometric lithography, Spindt cone deposition, and integrated with additional metallization layers and conventional lithography to create discrete arrays for electrical characterization. The fabricated cones have similar size and structure to those simulated, Figure 21.

Electrical characterization of the 100 nm aperture (200 nm tip to tip spacing) has shown that arrays can operate at voltages as low as 16 volts and provide adequate current to support flat panel display applications. A variation of 10,000:1 in emission current can be controlled by small variations in the gate voltage of a MOSFET demonstrating the feasibility of using low voltage driver voltages. The above demonstration has gone a long way to show the feasibility of a high brightness, high resolution FEA image sources for head-mounted displays. The objectives for the next year are to fabricate arrays with a 100 nm aperature using a Si etch back technique, and a CMP defined poly-silicon gate.

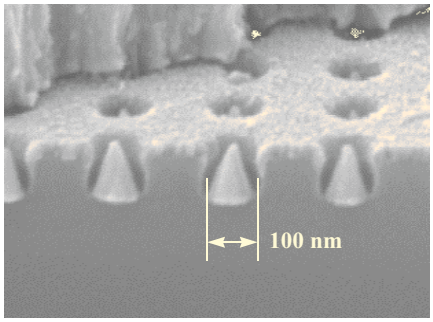

Fig. 21: 100 nm gate aperture molybdenum field emitter cones with chromium gate formed with using a vertical evaporation.

High-Dispersion, High Efficiency Transmission Gratings for Astrophysical X-ray Spectroscopy

Personnel

R. C. Fleming, P. Hindle, M. McGuirk, E. Murphy, Dr. M. L. Schattenburg (C. R. Canizares, H. I. Smith)

Sponsorship

NASA

Through a collaboration among the Center for Space Research (CSR), the Nanostructures Laboratory (NSL), and the Microsystems Technology Laboratories (MTL), x-ray transmission gratings are fabricated for the NASA Advanced X-ray Astrophysics Facility (AXAF) x-ray telescope, scheduled for launch on the Space Shuttle in 1999. This major national facility will provide high-resolution imaging and spectroscopy of x-ray-emitting astrophysical objects, with unprecedented power and clarity, promising to significantly widen our view of the Universe.

Many hundreds of large-area, gold transmission gratings, with 200 nm and 400 nm periods, are required for the High-Energy-Transmission-Grating Spectrometer (HETGS) on AXAF, which will provide high-resolution x-ray spectroscopy in the 100 eV to 10 keV band. In order to achieve spectrometer performance goals, the gratings need to have very low distortion (< 200 ppm), and high-aspect-ratio structures, significantly pushing the state-of-the-art of nanofabrication.

The need for high grating quality, and an aggressive production schedule, demanded the development of a robust, high-yield manufacturing process. We adopted a scheme involving interferometric lithography with tri-level resist, followed by cryogenic reactive-ion etching and gold electroplating (see Figure 24). A chemical etching step then yields membrane-supported gratings suitable for space use. The gratings underwent extensive testing before being assembled in the spectrometer.

A cleanroom fabrication facility was constructed (the Space Microstructures Laboratory, on the 4th floor of Building 37 adjacent to the Gordon Stanley Brown Building), in order to fabricate the AXAF gratings. The proximity of the lab to the MTL allowed the sharing of many services, such as DI and process water, nitrogen, process vacuum, and waste drains. The SML space includes 1700 sq-ft of Class 100 clean room and associated support areas, and a large complement of state-of-the-art equipment.

Production of flight gratings and spares has been completed, and the fully assembled and calibrated HETGS flight instrument (see Figure 25) has been integrated with the AXAF spacecraft which is now undergoing final test prior to launch.

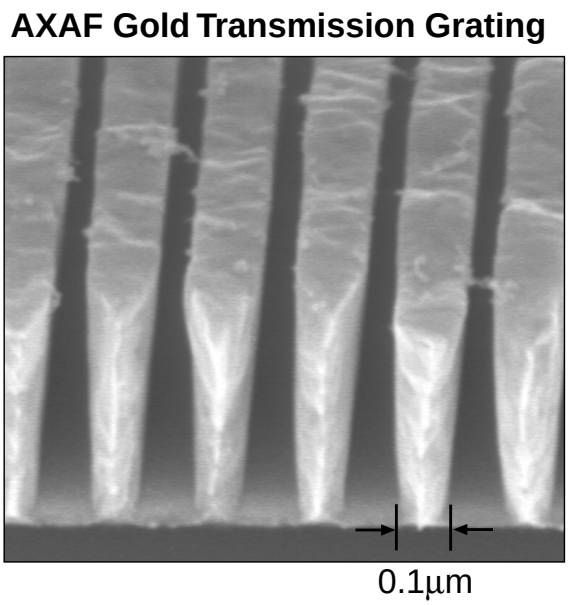

Fig. 24: Scanning-electron micrograph of a 200 nm-period gold x-ray transmission grating, cleaved to show the sidewalls of 100 nm wide lines.

continued

Transmission Gratings as UV-blocking Filters for Neutral Atom Imaging

Personnel

R. C. Fleming, P. Hindle, M. McGuirk, E. Murphy,
(M. L. Schattenburg, C. R. Canizares, H. I. Smith)

Sponsorship

Los Alamos National Laboratory
Southwest Research Institute

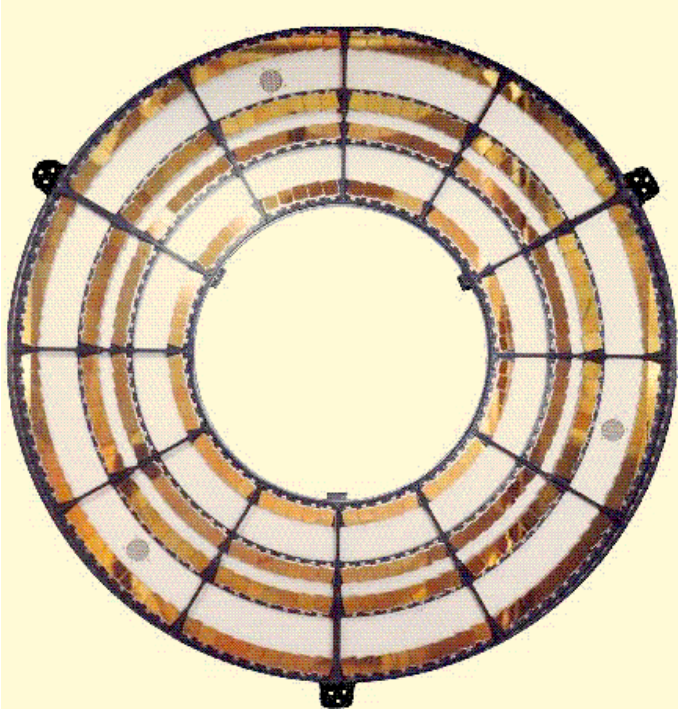

Fig. 25: Photograph of the HETGS flight instrument, which consists a 1.0 meter-diameter aluminum wheel populated with hundreds of 200 nm and 400 nm-period gold x-ray transmission gratings (340 total).

Neutral-atom-beam imaging detectors are used to study dilute plasmas in laboratory systems such as Tokamaks, and in astrophysical environments such as the magnetospheric region of the Earth. Neutral atom emission can be a particularly useful probe of plasmas since neutrals travel in straight lines-of-sight, unperturbed by electromagnetic fields.

Charge-exchange interactions between Solar-wind particles and atoms in the Earth's tenuous outer atmosphere are predicted to form strong currents of neutral atoms (mostly oxygen and helium) emanating from the Earth, which, if they could be imaged, would provide unprecedented real-time mapping of this complicated magnetohydrodynamic environment. This information would be valuable in order to safeguard the health of orbiting satellites, and ensure the stability of our nation's electric power grid.

Unfortunately, sensitive orbiting neutral-beam detectors are easily overwhelmed by the bright flux of UV photons typically emitted from astrophysical plasmas (mostly the 121.6 nm emission from hydrogen and the 58.4 nm emission from helium). Filters which allow the passage of low-energy neutral atoms but block UV light are essential for the performance of this instrumentation. Through several years of collaboration with the Los Alamos National Laboratory (LANL), the University of West Virginia, the University of Southern California, and the Southwest Research Institute (SwRI), we have developed neutral beam filters which consist of mesh-supported, 200 nm-period, gold transmission gratings with 30-60 nm wide slots, shown in Fig. 27. The tall, narrow slots in the gratings behave as lossy waveguides at or below cutoff, providing UV discrimination on the order of millions (See Fig. 26).

We have been awarded contracts by LANL and SwRI to deliver a quantity of flight grating filters for the Medium Energy Neutral Atom (MENA) instrument on the NASA

continued

Magnetospheric Imaging Medium-Class Explorer (IMAGE) mission, scheduled for launch in January 2000.

We anticipate shortly a new LANL contract to fabricate improved gratings for the NASA Two Wide-Angle Imaging Neutral-atom Spectrometers (TWINS) Mission.

The gratings are fabricated by interferometric lithography with tri-level resist, followed by cryogenic reactive-ion etching and gold electroplating. An additional masking step followed by nickel plating fabricates the mesh support structure, and a final chemical etching step yields mesh-supported gratings suitable for space use.

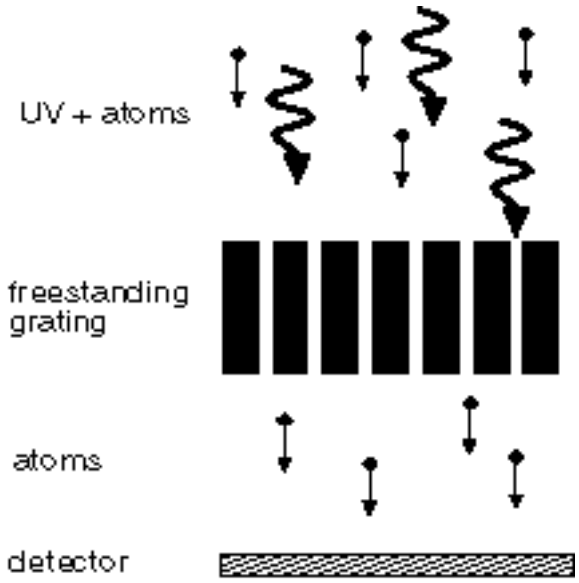

Fig. 26: Concept of UV filtering by means of a metal freestanding grating. As a result of polarization and waveguide effects, UV is blocked while allowing the passage of atoms. In this way, UV background counts on the atom detector are avoided.

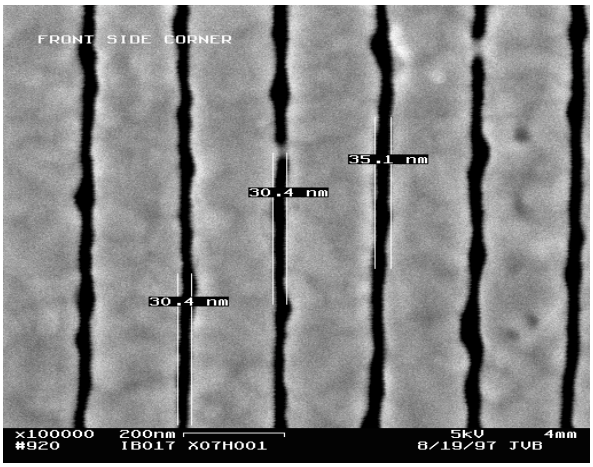

Fig. 27: Scanning-electron micrograph image showing a close up of the UV blocking grating. Due to the narrow slot width of 30-35 nm, as shown in the picture, and the large slot depth (~500 nm), the UV transmission is extremely low (10^{-6} to 10^{-7} at 121.6 nm), while decreasing the transmitted atomic flux only by a factor of 10.

Super-smooth X-ray Reflection Gratings

Personnel

C. Chen, R. C. Fleming, P. Hindle, M. McGuirk, E. Murphy (M. L. Schattenburg, C. R. Canizares, H. I. Smith)

Sponsorship

NASA

Grazing-incidence x-ray reflection gratings are an important component of modern high-resolution spectrometers and related x-ray optics. These have traditionally been fabricated by diamond scribing with a ruling engine, or more recently, by interferometric lithography followed by ion etching. These methods result in gratings which suffer from a number of deficiencies, including high surface roughness and poor groove profile control, leading to poor diffraction efficiency and large amounts of scattered light.

We are developing improved methods for fabricating blazed x-ray reflection gratings which utilize special (111) silicon wafers, cut ~1 degree off the (111) plane. Silicon anisotropic etching solutions, such as potassium hydroxide (KOH), etch (111) planes extremely slowly compared to other crystallographic planes, resulting in the desired super-smooth blaze surface. Previous work used similar off-cut (111) silicon substrates to fabricate blazed diffraction gratings. However, that method utilized a second KOH etch step which compromised the grating facet flatness and is unsuitable for small grazing-angle x-ray diffraction.

Our gratings are patterned using interferometric lithography with the 351.1 nm wavelength, and transferred into the substrate using tri-level resist processing, reactive-ion etching (RIE), and silicon-nitride masking during the KOH etch. The narrow (~0.1 μm) ridge of silicon which supports the nitride mask is removed using a novel chromium lift-off step followed by a CF_4 RIE trench etch. The result is extremely-smooth sawtooth patterns, which, after applying a thin evaporative coating of Cr/Au, are suitable for x-ray reflection (see Figure 28). Gratings have been tested with special x-ray spectrometers in the laboratories of our collaborators at Columbia University and the Lawrence Berkeley National Laboratory. Peak gratings efficiencies achieved are ~35% greater than those of the best available ruled masters of comparable design (see Figure 29).

Fig. 28: (a) An AFM image of a traditional mechanically-ruled and replicated x-ray reflection grating (Bixler et al., Proc. SPIE 1549 , 420-428 [1991]). Note the rough, wavy grating surfaces which lead to poor diffractive performance. (b) An AFM image of a blazed x-ray reflection grating fabricated by anisotropic etching of special off-cut (111) silicon wafers. Note the improvement of grating surface flatness and smoothness, leading to significantly improved performance.

continued

continued

Submicron-Period Transmission Gratings for X-Ray and Atom-Beam Spectroscopy and Interferometry

Personnel

J. M. Carter, J. M. Daley, E. Murphy, T. A. Savas, (M. L. Schattenburg, H. I. Smith)

Sponsorship

ARO, X-OPT, Inc.

Potential applications of these improved gratings are for laboratory and satellite-based high-resolution x-ray spectroscopy. The current phase of the work involves patterning gratings on super-flat wafers, and trimming the substrates into the desired rectangular format.

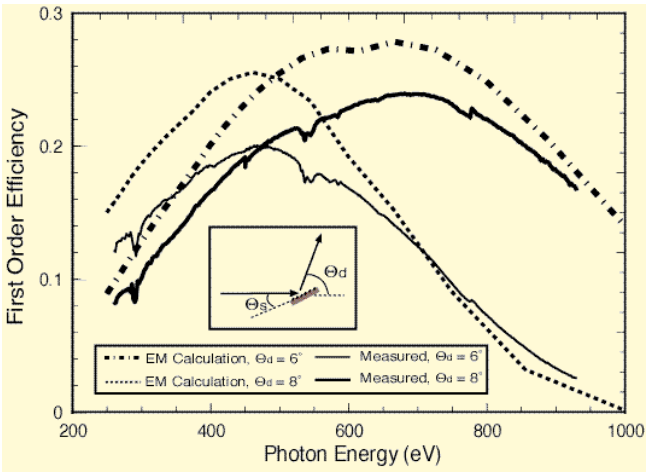

Fig. 29: Comparison of x-ray diffraction efficiency measured at Lawrence Berkeley Laboratory and electromagnetic finite element calculations performed at Columbia University. Peak gratings efficiencies achieved are ~35% greater than those of the best available ruled masters of comparable design.

Transmission gratings with periods of 100 to 1000 nm are finding increasing utility in applications such as x-ray, vacuum-ultraviolet, and atom-beam spectroscopy and interferometry. Over 30 laboratories around the world depend on MIT-supplied gratings in their work. For x-ray and VUV spectroscopy, gratings are made of gold and have periods of 100 to 1000 nm, and thicknesses ranging from 100 to 1000 nm. The gratings are most commonly used for spectroscopy of the x-ray emission from high-temperature plasmas. Transmission gratings are supported on thin (1 micron) polyimide membranes, or made self supporting ("free standing") by the addition of crossing struts (mesh). (For short x-ray wavelengths, membrane support is desired, while for the long wavelengths, a mesh support is preferred in order to increase efficiency.) Fabrication is performed by interferometric lithography combined with reactive-ion etching and electroplating. Progress in this area tends to focus on improving the yield and flexibility of the fabrication procedures.

Another application is the diffraction of neutral-atom and molecular beams by mesh supported gratings. Lithographic and etching procedures have been developed for fabricationg free-standing gratings and grids in thin silicon nitride (SiNx) membranes supported in a Si frame. Figure 30 shows a free-standing 100 nm period grating in 100 nm-thick silicon nitride. Figure 31 shows a 100 nm-period grid in a 100 nm-thick SiNx membrane. Such a grid is used in experiments as a "molecular sieve."

We have established a collaboration with the Max-Planck Institute in Goettingen, Germany, in which they utilize our gratings and grids of 100 nm period in diffraction experiments using He atom beams. Figure 32 shows a spectrum obtained by diffracting a He beam through a 100 nm-period transmission grating. Figure 33 shows the transmission of a grating as a function of helium-beam incident angles. Data obtained by He diffraction at

continued

continued

large incident angles showed Lyman ghosts in the spectrum. This data led to the development of new fabriction techniques to improve the quality of the free-standing gratings in silicon nitride. Diffraction spectra from gratings made with the improved process show no Lyman ghosts, illustrating the important synergy between applications and nanofabrication.

In addition, we have established a collaboration with Professor David E. Pritchard at MIT. His group uses our 100 nm-period gratings in diffraction and interferometer experiments with neutral sodium atom beams.

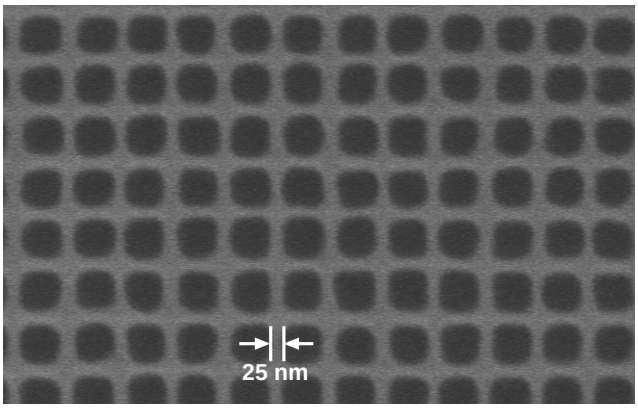

Fig. 30: Scanning electron micrograph of a free-standing 100 nm-period grating (50 nm-wide bars) in a silicon nitride membrane of area 500 microns by 5 mm.

Fig. 31 Scanning electron micrograph of a free-standing 100 nm period grid in a silicon nitride membrane of area 500 micron by 5 mm. Such grids are used in experiments to separate out Helium trimers from other clusters.

continued

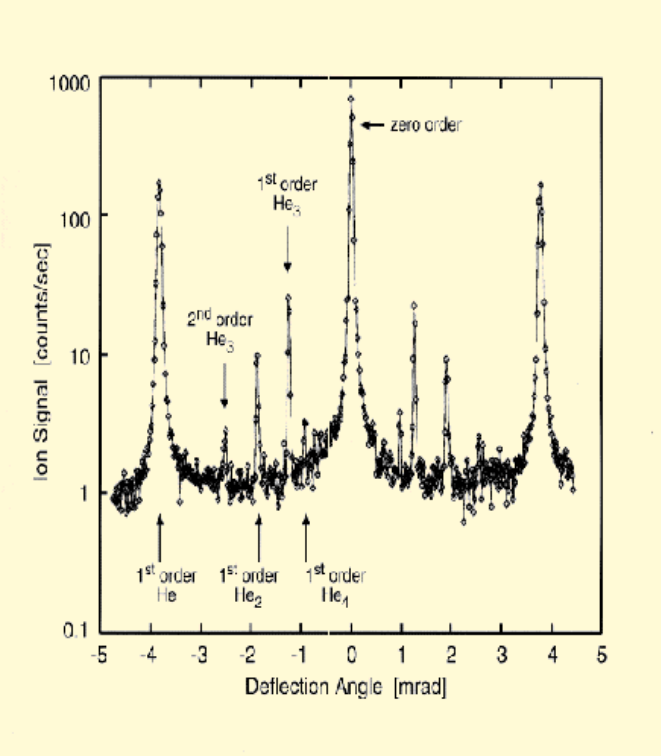

Fig. 32: Helium beam diffraction spectrum. These results were obtained by Wieland Schoellkopf and Peter Toennies at the Max-Planck Institute in Goettingen, Germany, using a grating such as in Figure 30.

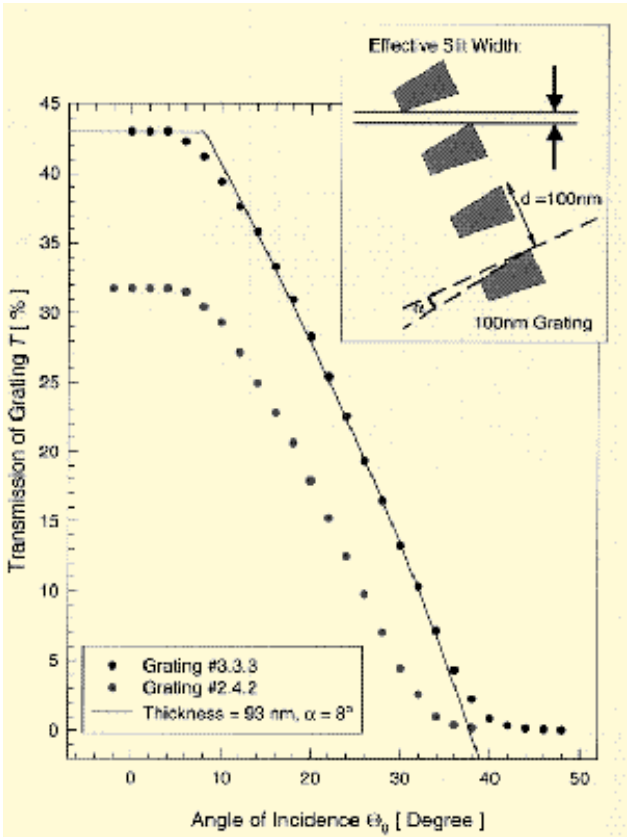

Fig. 33: Measured total transmitted intensity through a 100 nm-period free-standing grating as a function of incident angle for a He atom beam. The line is a fit assuming a truncated wedge shape for the cross section of the grating bars, as depicted in the inset. Analysis indicated a grating thickness of 93 nm and a wedge angle of 8 degrees.